Indian Journal of Pure & Applied Physics
Vol. 63, March 2025, pp. 212-223
DOI: 10.56042/ijpap.v63i3.11797

Theoretical Investigation of Relativistic Electrons in DT, D^3He, and $P^{11}B$ Fusion Plasma using ICF Approach

S N Hosseinimotlagh* & A Shakeri
Department of Physics, Shiraz Branch, Islamic Azad University, Shiraz, Iran

Received: 13 June 2024; accepted: 11 March 2025

The study of ICF is important and requires a long time due to the various physical phenomena. One of the phenomena is the interaction potentials between ions and electrons that can provide the possibility of studding the fusion plasma more accurate. Dynamic properties of dense plasma enables us to evaluate the thermonuclear reaction parameters more accurately. In general, in this work we were able to investigate the role of relativistic electrons in DT, D^3He, and $P^{11}B$ fusion plasma using ICF approach in terms of temperature, distance, and Lorentz factor. The results of our calculations show that the calculated parameters in our work for the DT fusion fuel are in good agreement with the results of other groups, which shows the validity of our research work. While for the parameters belong to D^3He and $p^{11}B$ fuels no references were found for comparison, because they have been studied for the first time by the authors of this article. It is hoped that this work can be a foundation for further research of aneutronic fuels.

Keywords: Plasma, Aneutronic, Effective interaction potential, Scattering, Temperature

1 Introduction

Nuclear fusion can be accomplished in various approaches, provided the fuel is compressed to a sufficient density and heated to an adequate temperature for enough time. However, two main experimental approaches, magnetic confinement fusion (MCF)[1,2] and inertial confinement fusion (ICF), have received more recognition for developing fusion technology[3,4]. Compared to the other energy sources, nuclear fusion has many advantages: no greenhouse gas or other pollutant emission during operations, no chain reactions, baseload production and load-following capabilities. These aspects make nuclear fusion extremely promising from the point of view of energy production, but it is not exempt from concerns and issues. In MCF, magnetic fields are a natural candidate for plasma confinement, because the electrically charged ions and electrons that make up the plasma interact with the magnetic field lines and follow well defined orbits, avoiding contact with the reactor walls. For example, Princeton fusion systems work based on MCF. The Direct Fusion Drive (DFD) proposed by Princeton Fusion Systems 12 (United States) is a compact fusion engine for space propulsion. The goal of DFD is to enable exploration missions in the Solar System[5-7]. The engine is designed to use D^3He fuel, exploiting a FRC to confine the plasma within a linear solenoid coil[8-9]. The DFD would be highly effective because it provides both propulsion and electricity production.

ICF exploits extremely high compressions of solid targets to bring the fuel up to ignition conditions ($n \sim 1025m{-}3$). Although some concepts exploit non-thermal acceleration of fuel ions up to suitable energies for fusion reactions, the most common approach is based on spherical pellets heated uniformly by laser beams. The energy burst ablates the outermost layer of the sphere, generating an inward shock wave that compresses the fuel, with a consequent fuel temperature increase up to 1–10 keV. The process takes place in extremely short times ($\sim 1 - 10$ ns) and the plasma confinement is not improved by the presence of external magnetic fields. The very short confinement time is indeed traded off by the high fuel density. Key enabling technologies for IFC are high-power lasers, highly efficient lasers, and fuel pellets, even though the extension to a power plant requires an effective breeding blanket design that must suit the radically different design of ICF devices. Contributions of paramount importance for ICF advancements, including the first ignited plasma ever achieved, have been provided by the National Ignition Facility (NIF)[10]. Additional experimental facilities investigating ICF are OMEGA (US)[11], and Gekko (Japan)[12] .

*Corresponding author:
(E-mail: nasrinhosseinimotlagh@gmail.com)

The most studied nuclear fusion reactions for energy applications are those employing as reactants1 a plasma of the isotopes of hydrogen (deuterium and tritium), ^{3}He or ^{11}B: D + T → $^4_2$He + n (17.6 MeV) , D + $^3_2$He → $^4_2$He + p (18.3 MeV) , and p + $^{11}_5$B → 3$^4_2$He (8.68 MeV). Any device that exploits fusion reactions requires fuel (and refueling). One of the important issue in fusion plasma is thermodynamical parameters of DT, D^{3}He, and P^{11}B fusion fuels using the interaction potential of fusion particles. Therefore, the main purpose of this article is to study this point. Therefore, in line with this goal, the paper is structured as follows: Section 2 introduces the main nuclear fusion fuels which are used in fusion reactors; Section 3 provides a theoretical investigation of relativistic electrons in fusion plasmas; Section 4 discusses extensively the main achievements of thermodynamics and dynamical properties of dense fusion plasma via inertial confinement fusion and finally the summery is given.

2 Nuclear Fusion Fuels

Fuel can be provided as a gas or as a solid pellet, usually stored and processed in loco. For p^{11}B fusion, both the reactants are abundant, but this is not the case for DT or D^{3}He fusion. Deuterium can be easily extracted from water, while tritium is a radioactive isotope with a half-life of 12.3 years (meaning that hardly any T is available in nature), and ^{3}He is an extremely rare element on the Earth. DT fusion devices are therefore being designed to produce (breed) tritium in the reactor itself by exploiting the nuclear reactions between neutrons and lithium. The component devoted to tritium breeding is the breeding blanket. Each DT fusion reaction produces a neutron, which travels almost freely through the plasma until reaching the structure surrounding the vacuum chamber, where the breeding blanket is located. Most of the neutrons are slowed down in the blanket, releasing energy in the form of heat and eventually being absorbed by the blanket materials. Materials with a high content of lithium are used to breed tritium according to the reactions : ^{6}Li + n → T + ^{4}He (4.8 MeV) and ^{7}Li + n → T + ^{4}He + n′ (–2.5 MeV).

^{3}He is instead produced by DD reactions or by tritium decay. In principle, a D^{3}He fusion device does not require a breeding blanket because it relies on an open fuel cycle, removing the complexity of a breeding blanket from the reactor design but introducing the need of an external source of ^{3}He. A large source of ^{3}He is found in Moon regolith. Many analyses have been carried out on the feasibility of 3He mining from the Moon, but only conceptual designs and missions have been produced so far because of the high financial risk of the projects and lack of validated technologies.

Boron is much more common than T or ^{3}He on the Earth. The main reserves are in Chile, China, Russia, and in the US. No supply issues are foreseen in the next future at the current rate of consumption. P^{11}B energy pursues non-thermal p^{11}B fusion by a combination of ultra-high acceleration of plasma blocks in a solid target and ultra-high magnetic fields (~10 kT) by high-power lasers. The solid target is a small cylinder of hydrogen and boron placed in a capacitive coil. Two lasers are required to reach ignition conditions. A first laser hits the target, while a second laser produces the ultra-high magnetic field by interaction with the capacitor coil[13]. Several experiments have been carried out to investigate the basic principles of non-thermal fusion[14], the interaction between PW-scale lasers with fuel block[15] and the optimal scheme (bulk vs. pitcher-catcher)[16], and the existence of an avalanche reaction in the fuel target[17]. Direct electricity generation is foreseen by decelerating the alpha particles exploiting a high voltage spherical shell in which the target and the coil are located. No fusion power plant is planned for the near future, but a roadmap highlighting the most important steps (e.g., numerical analysis of capacitor coil magnetic field, behavior of materials under kT magnetic fields, improvement of PW-class lasers) to achieve power production from p^{11}B fusion reactions has been developed[18]. The fusion cross section for the aforementioned reactions is reported in Figure 1 as a function of the energy.

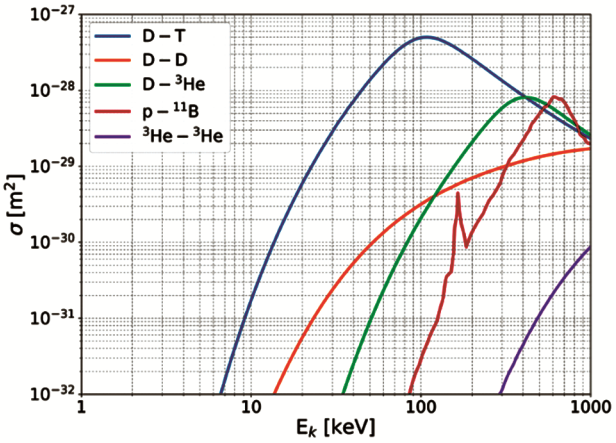

Fig. 1 — Experimental cross sections (σ) for the most relevant fusion reactions

3 Theoretical Investigation of Relativistic Electrons in Fusion Plasmas

One of the basic problems in plasma physics is the interaction and energy loss of charged particles in plasma[19, 20]. This issue usually emphasizes ions (protons, alphas, etc.) in the field of heating and ignition, through ICF and internal explosion[21-23]. The concept of fast ignition through ICF considers the energy deposition of relativistic fast electrons in non-isothermal dense hot plasmas of DT, D^3He and $P^{11}B$ and preheated fuel[24, 25]. The scattering effects are key points for quantitative evaluation of preheated fuel. The starting point of these calculations includes the examination of the relativistic elastic differential cross sections for the scattering of fully ionized electrons and ions with charge Z[26, 27]. Such that these relativistic elastic differential cross sections for electron-ion and electron-electron scattering are estimated by Eqs (1) and (2), respectively[28,29]:

$$\left(\frac{d\sigma}{d\Omega}\right)^{ei} \approx \frac{z^2}{4}\left(\frac{r_0}{\gamma\beta^2}\right)^2 \frac{1}{\sin^4 \theta/2} \quad \ldots (1)$$

$$z\left(\frac{d\sigma}{d\Omega}\right)^{ee} \approx z\frac{(\gamma+1)^2}{\left(2\sqrt{(\gamma+1/2)}\right)^4}\left(\frac{r_0}{\gamma\beta^2}\right)^2 \frac{1}{\sin^4 \theta/2} \quad \ldots (2)$$

where $\beta = \frac{v}{c}$, $\gamma = \left(1-\beta^2\right)^{\frac{-1}{2}}$ and r_0 is the classical electron radius, which is follows from the relation: $r_0 = \frac{e^2}{m_0 c^2}$. The ratio of the differential scattering cross sections of relativistic electron-electron to electron-ion is represented by $\Re$ (Equ. (3)).

$$\Re = Z\left(\frac{d\sigma}{d\Omega}\right)^{ee} \Big/ \left(\frac{d\sigma}{d\Omega}\right)^{ei} \approx \frac{(\gamma+1)^2}{\left(2\sqrt{(\gamma+1/2)}\right)^4}\frac{1}{Z} \quad \ldots (3)$$

In Fig. 2, we have drawn the two-dimensional diagram of $\Re$ variations in terms of γ for three fusion reactions a) DT, b) D^3He and c) $P^{11}B$.

From the observation of Fig. 2, it can be seen that with the increase of the Lorentz factor γ, first R increases and then it has a decreasing trend such that DT has the highest value but $P^{11}B$ has the lowest value. To calculate the effects of multiple scattering, the Boltzmann scattering equation according to Eq (4) is used[30]:

$$\frac{\partial f}{\partial s} + V \cdot \nabla = n_i \int [f(X.V.'S) - f(X.V.S)]\, \sigma(|V - V'|) dV' \quad \ldots (4)$$

where f is the angular distribution function of scattered electrons, n_i represents the numerical density of plasma ions with charge Z and X represents the direction in which scattering occurs and $s = \sigma_1(E)$, and $\sigma_1(E)$ means the cross-sectional area of total scattering, which follows the Eq (5):

$$\sigma_1(E) = \sigma_1^{ei}(E) + Z\sigma_1^{ee}(E) = 4\pi n_i \left(\frac{r_0}{\gamma\beta^2}\right)^2 \left[Z^2 \ln\Lambda^{ei} + \frac{(\gamma+1)^2}{\left(2\sqrt{(\gamma+1/2)}\right)^4} Z \ln\Lambda^{ee} \right] \quad \ldots (5)$$

In Fig. 3 we presented the variations of $\sigma_1(E)$ (total scattering cross section) in terms of γ and T in the range of $0 \cdot 01 \le \gamma \le 10$ and $1 \le T(keV) \le 300$.

In Equation 5, which is the equation related to $\sigma_1(E)$, the two quantities σ_{ei} and σ_{ee} are electron-ion and electron-electron scattering cross sections, respectively, where: $\sigma_{ei} = \int (d\sigma/d\Omega)^{ei}\, d\Omega$ and $\sigma_{ee} = \int (d\sigma/d\Omega)^{ee}\, d\Omega$ (Figs 4 & 5). These figures show the two and three-dimensional variations of s(E) (the total length of the path traveled by plasma particles) in terms

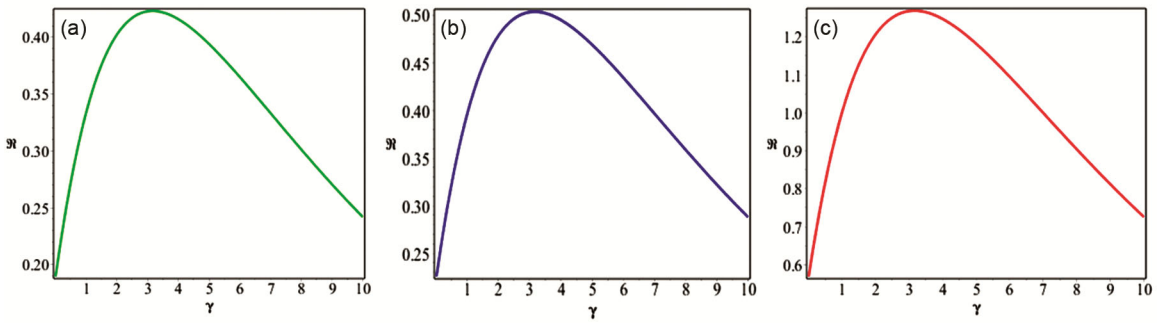

Fig. 2 — Comparison of $\Re$ (the ratio of the differential elastic cross sections of electron-electron to electron-ion scattering) variations in terms of γ for three fusion reactions a) DT, b) D^3He and c) $P^{11}B$

of γ for three reactions a) DT, b) D^3He and c) $P^{11}B$ in the range of 0·01≤γ≤10 and 1≤T(keV)≤300 and the two-dimensional variations of σ_{ee} and σ_{ei} variations in terms of γ ($\sigma = \sigma_1(E)$), respectively.

According to the above figures, our calculations show that the variations of the total scattering cross-section ($\sigma_1(E)$) and the variations of the electron-electron and electron-ion scattering cross-section in terms of Lorentz coefficient γ and temperature T, at different temperatures, initially have fixed values, but with increasing γ, at first increases and reaches its maximum value at γ≃1 and then decreases and the variations of s(E) (the total length of the path traveled by the plasma particles) also decreases with increasing temperature but increases with increasing γ and has the highest value in order of DT, then D^3He and finally $P^{11}B$. Also, in equation (5), Λ^{ei} and Λ^{ee} are known as the Coulomb logarithms of electron-ion and electron-electron, respectively, which are determined by the relations $\Lambda^{ei} = \lambda_D/b^{ei}_{min}$ and $\Lambda^{ee} = \lambda_D/b^{ee}_{min}$.

In the equations of ln Λ^{ei} and ln Λ^{ee}, λ_D is called Debye length and follows the relation $\lambda_D = \left(\frac{\varepsilon_0 T}{ne^2}\right)^{\frac{1}{2}}$ where ε_0 is the vacuum permeability.

Also, b^{ei}_{min} and b^{ee}_{min} are the minimum electron-ion and electron-electron collision parameters, respectively, which are defined by the relations

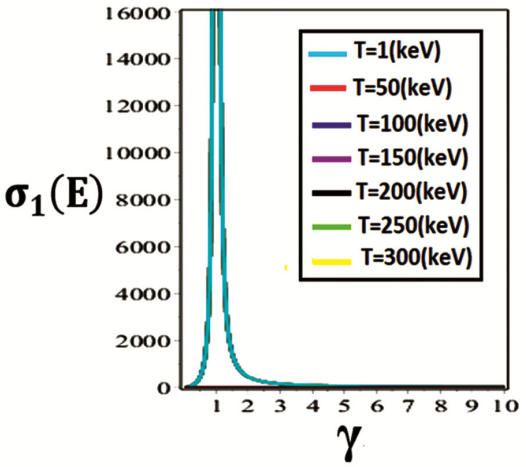

Fig. 3 — variations of $\sigma_1(E)$ (total scattering cross-section) as a function of γ and T

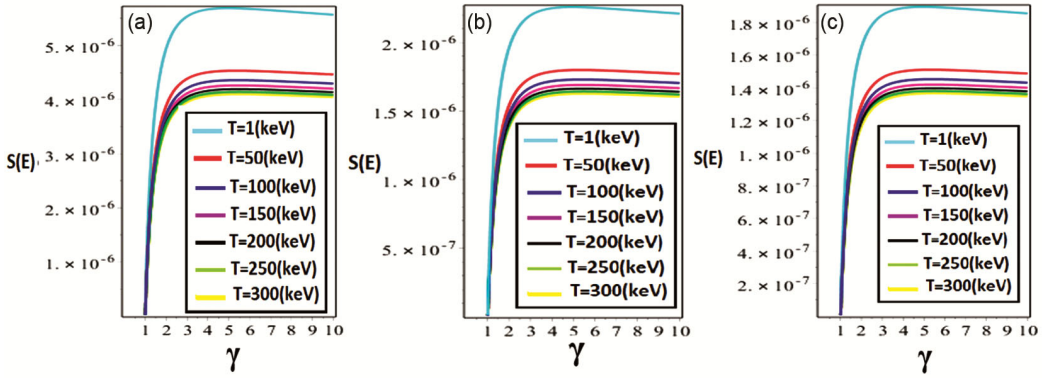

Fig. 4 — variations of s (E) as a function of γ and T in the range of 0 01≤γ≤10 and 1≤T (keV) ≤ 300, for three fusion reactions a) DT, b) D^3He, and c) $P^{11}B$

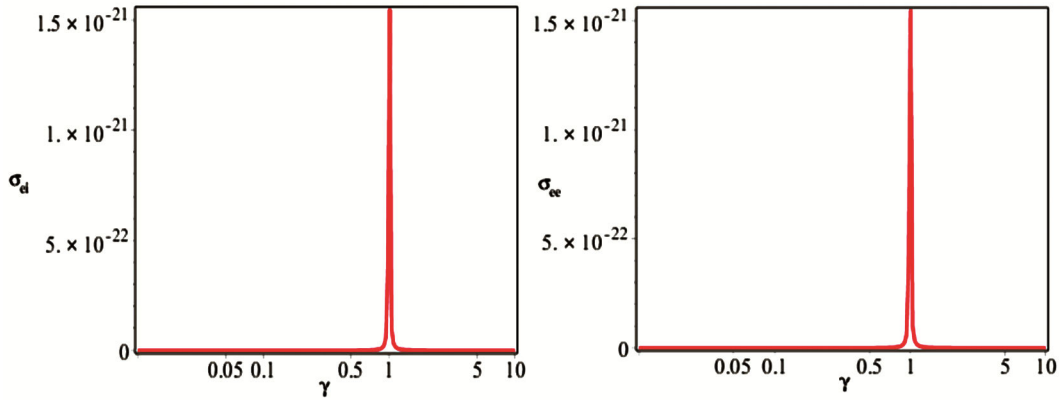

Fig. 5 — variations of σ_{ee} and σ_{ei} as a function of γ

$$b_{min}^{ei} = \frac{Zr_0}{\gamma\beta^2} \text{ and } b_{min}^{ee} = 2(\gamma+1)r_0 \Big/ \left[\left(2\sqrt{\left(\gamma+1/2\right)}\right)^2 \gamma\beta^2\right].$$

Equation (4) has been solved in cylindrical coordinates with the assumption that the scattering is symmetric. The solution that satisfies the boundary conditions is in the form of Eq (6)[31]:

$$f(\theta.S) = \frac{1}{4\pi}\sum_{l=0}^{\infty}(2l+1)\ P_l(\cos\theta)\ \exp\left[-\int_0^s \sigma_1(s')\,ds'\right] \quad \ldots(6)$$

where $P_l(\cos\theta)$ is Legendre's polynomial. Using the orthogonality condition and considering l=1, $\langle\cos\theta\rangle$ can be obtained by equation (7) where $\langle\cos\theta\rangle$is the average angle of multiple scattering:

$$\langle\cos\theta\rangle = \int f(\theta.s)P_1(COS\theta)d\Omega = \exp\left[-\int_0^s s'\,ds'\right] = \exp\left[-\int_{E_0}^{E}(s')\left(\frac{dE}{ds}\right)^{-1}dE\right] \quad \ldots(7)$$

In Fig. 6, we have drawn the variations of $\langle\cos\theta\rangle$ (average multiple scattering angle) in terms of γ and T in the range of 0·01≤γ≤10 and 1≤T(keV)≤300.

From the observation of Fig. 6, it is clear that the variations of average angle of multiple scattering ($\langle\cos\theta\rangle$) in terms of the Lorentz coefficient γ and temperature T are almost constant at different temperatures, and with increasing γ, it increases rapidly and reaches a constant value. $\langle\cos\theta\rangle$ relates dE/ds to dE/dx by Eq (8) where dE/ds is stopping power along the path and dE/dx is the linear stopping power[32]:

$$\frac{dE}{dx} = \langle\cos\theta\rangle^{-1}\frac{dE}{ds} \quad \ldots(8)$$

In fact, the stopping power comes from interactions with plasma electrons and plasma fluctuations. The stopping power during the path follows the Eq (9):

$$\frac{dE}{ds} = -\frac{2\pi r_0^2 m_0 c^2 n_i Z}{\beta^2}\left\{\ln\left[\frac{(\gamma-1)\lambda_D}{2\sqrt{2\gamma}r_0}\right]^2 + 1 + \frac{1}{8}\left(\frac{\gamma-1}{\gamma}\right)^2 - \left(\frac{2\gamma-1}{\gamma}\right)\ln 2 + \ln\left(\frac{1\cdot 123\beta}{\sqrt{2\,kT_e/m_0c^2}}\right)^2\right\} \quad \ldots(9)$$

In Figs 7 and 8, we have drawn the variations of dE/ds (stopping power along the path) in terms of γ and T for three fusion reactions a) DT, b) D^3He and c) $P^{11}B$ in the range of 0·01 ≤γ≤10 and 1≤T(keV)≤300.

From the observation of Fig. 7 and the calculations we have made for the variations of stopping power during the path (dE/ds) for the three fusion reactions DT, D^3He and $p^{11}B$ in terms of γ and T, it can be

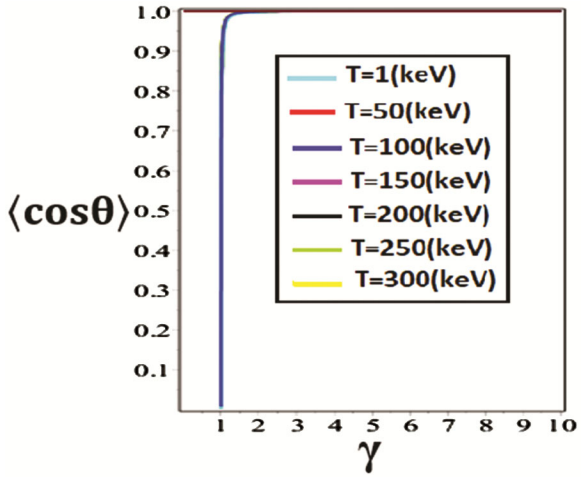

Fig. 6 — variations of $\langle\cos\theta\rangle$ as a function of γ and T

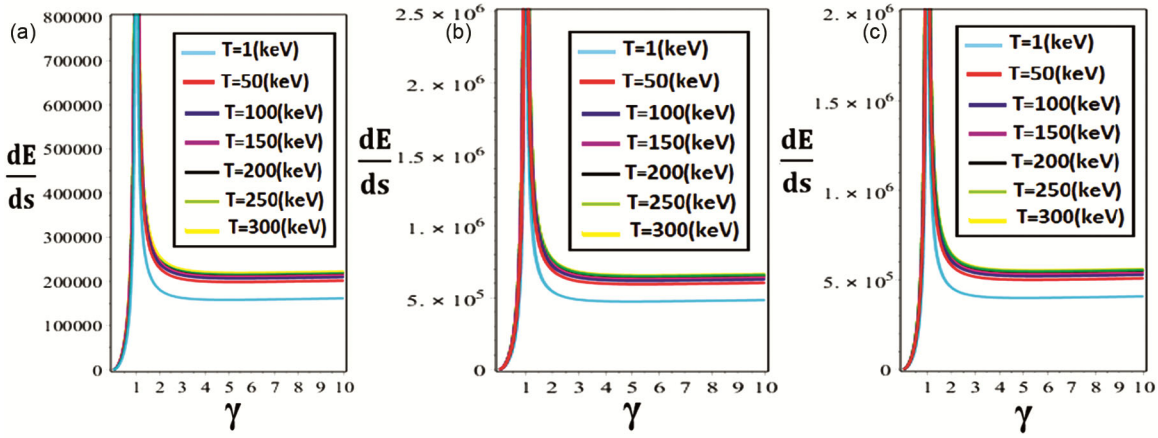

Fig. 7 — variations of $\frac{dE}{ds}$ as a function of γ and T for three fusion reactions: a) DT, b) D^3He, and c) $P^{11}B$ in the range of 0. 01 ≤ **γ** ≤ 10 and 1 ≤ T (keV) ≤300

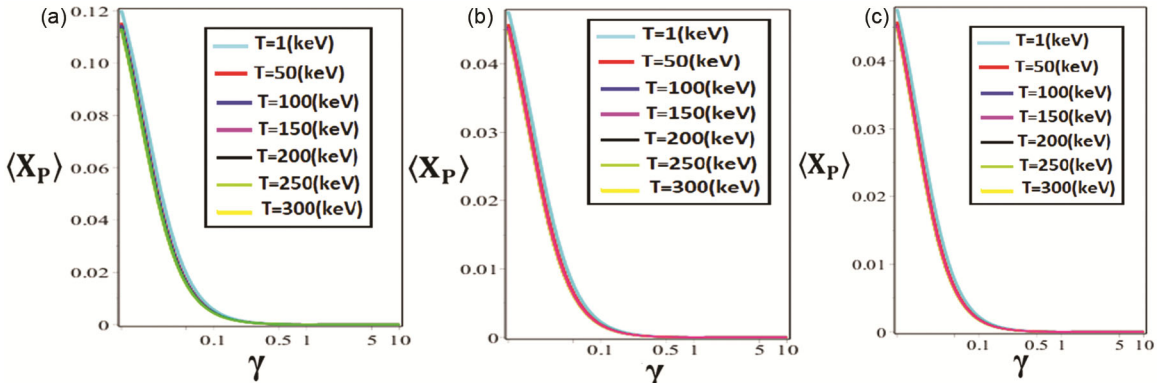

Fig. 8 — two and three-dimensional variations of $\langle X_P \rangle$ as a function of γ and T for three fusion reactions: a) DT, b) D^3He, and c) $P^{11}B$ in the range of 0. 01 ≤ γ ≤ 10 and 1 ≤ T (keV) ≤300

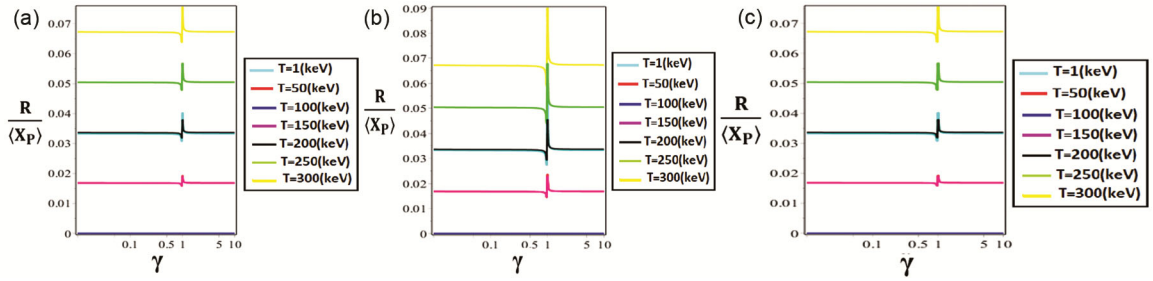

Fig. 9 — variations of $\frac{R}{\langle X_P \rangle}$ as a function of γ and T for three fusion reactions: a) DT, b) D^3He, and c) $P^{11}B$ in the range of 0·01≤γ≤10 and 1 ≤T (keV) ≤300

concluded that with increasing temperature, the dE/ds value increases and reaches its maximum value at γ≃1 and then has a decreasing trend and has the maximum value firstly $P^{11}B$, then D^3He and finally DT. The linear stopping power, i.e., dE/dx, is a result of the effects of multiple scattering, where β and γ are relativistic conditions that are related to $\beta = \frac{v}{c}$ and $\gamma = (1-\beta^2)^{\frac{-1}{2}}$ respectively. The total length of the path that the electrons travel during scattering and finally become thermal is represented by R and is obtained from equation (10):

$$R = \int_0^R ds' = \int_{E_0}^{\sim KT} \left(\frac{dE}{ds}\right)^{-1} dE \qquad \ldots (10)$$

The average distance traveled along the primary path of the electron (or penetration depth) is represented by $\langle X_P \rangle$, which is determined by equation (11):

$$\langle X_P \rangle = \sum_{n=0} e^{-n} \int_{E_n}^{E_{n+1}} \langle \cos\theta \rangle \left(\frac{dE}{ds}\right)^{-1} dE \qquad \ldots (11)$$

In Fig. 8, we have drawn the variations of $\langle X_P \rangle$ (penetration depth) in terms of γ and T for three reactions a) DT, b) D^3He and c) $P^{11}B$ in the range of 0·01≤γ≤10 and 1≤T(keV)≤300.

From looking at Fig. 8, we can see that the changes in penetration depth ($\langle X_P \rangle$) for the three fusion reactions DT, D^3He and $P^{11}B$ in terms of the Lorentz coefficient γ and temperature T are a constant value at different temperatures, but with increasing γ, it decreases and DT, D^3He and $P^{11}B$ have the highest value respectively. Also, the variations of the ratio of total length of the path that electrons travel during scattering and eventually become thermal, to the distance along the initial path of the electron (or penetration depth), i.e. $\frac{R}{\langle X_P \rangle}$, in terms of γ and T for three fusion reactions DT, D^3He and $P^{11}B$ in the range of 0·01≤γ≤10 and 1≤T(keV)≤300 are given in Fig. 9.

From observing the variations of $\frac{R}{\langle X_P \rangle}$ for the three fusion reactions of DT, D^3He and $P^{11}B$ in terms of γ and T (Fig. 9), it is clear that the maximum value of $\frac{R}{\langle X_P \rangle}$ is related to DT, D^3He, and $P^{11}B$, respectively.

4 Thermodynamics and Dynamical Properties of Dense Fusion Plasma via Inertial Confinement Fusion

Knowing the dynamical and thermodynamics properties of dense plasma enables us to calculate and design the thermonuclear reaction more accurately. It

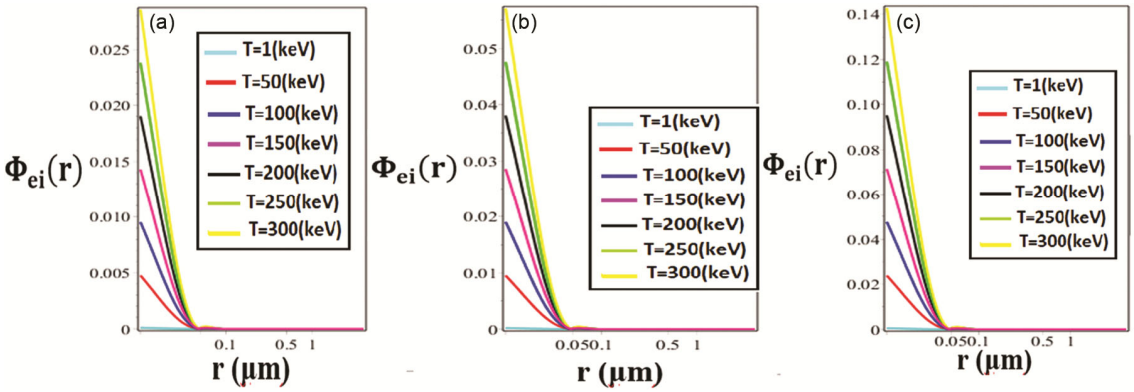

Fig. 10 — variations of $\mathbf{\Phi_{ei}(r)}$ (electron-ion effective interaction potential) as a function of r and T for the three fusion reactions: a) DT, b) D^3He, and c) $P^{11}B$ in the range of 0≤r (μm) ≤4 and 1≤T (keV) ≤300

is clear that considering the effective interaction potentials of particles is important for calculation of plasma properties. Therefore, these effective interaction potentials, which include charge screening effects at large distances as well as quantum mechanical effects at short distances, have been investigated in this article.

4.1 Effective Interaction Potentials

Since plasma particles interact with each other and with electrons, the interaction between them is characterized by the following effective interaction potential[33]:

$$\Phi_{\alpha\beta}(r) = \frac{Z_\alpha Z_\beta}{r\sqrt{1-(2\lambda_{\alpha\beta}/r_D)^2}}\left(\exp(-rB) - \exp(-rA)\right) \quad \ldots (12)$$

where α, β are the types of particles (ions or electrons) and Z_α, Z_β are the atomic numbers of α, β particles. The expression $\lambda_{\alpha\beta} = \hbar/\sqrt{4\pi m_{\alpha\beta} k_B T}$ is the thermal wavelength of both α and β particles and the expression $m_{\alpha\beta} = m_\alpha m_\beta/\left(m_\alpha + m_\beta\right)$ is related to the reduced mass, and r_D is the Debye radius and it is given by $r_D = \left(\frac{\varepsilon_0 T}{ne^2}\right)^{\frac{1}{2}}$. In Figures 10, 11 and 12, we plotted the variations of $\Phi_{ei}(r)$ (electron-ion effective interaction potential), $\Phi_{ee}(r)$ (electron-electron effective interaction potential) and $\Phi_{ii}(r)$ (ion-ion effective interaction potential) respectively, in terms of r and T for three fusion reactions a) DT, b) D^3He and c) $p^{11}B$ in the range of 0≤r(μm) ≤4 and 1≤T(keV)≤300. A and B follow Eqs (13) and (14), respectively:

$$B^2 = \frac{1}{2\lambda_{\alpha\beta}^2}\left(1 - \sqrt{1-\left(\frac{2\lambda_{\alpha\beta}}{r_D}\right)^2}\right) \quad \ldots (13)$$

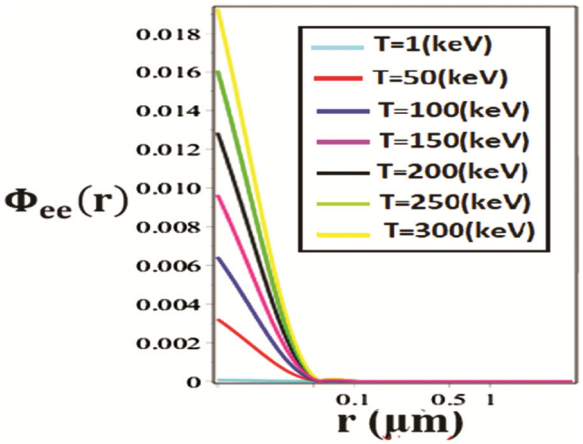

Fig. 11 — variations of $\mathbf{\Phi_{ee}(r)}$ (electron-electron effective interaction potential) as a function of r and T in the range of 0≤r (μm) ≤4 and 1≤T (keV) ≤300 for the three fusion reactions DT, D^3He, and $P^{11}B$

$$A^2 = \frac{1}{2\lambda_{\alpha\beta}^2}\left(1 + \sqrt{1-\left(\frac{2\lambda_{\alpha\beta}}{r_D}\right)^2}\right) \quad \ldots (14)$$

We have given the results of our calculations in Figs 10 -11. From their observation, we find that the variations of effective electron-ion interaction potential ($\Phi_{ei}(r)$) and the effective ion-ion interaction potential ($\Phi_{ii}(r)$) and the effective electron-electron interaction potential ($\Phi_{ee}(r)$) for all three fusion reactions DT, D^3He and $P^{11}B$ in terms of the interaction distance r and temperature T, such that at first all of mentioned interaction potentials increase and then decrease. Also, in Figure10, $P^{11}B$ has the maximum value of $\Phi_{ii}(r)$, , then D^3He, and finally DT. While in Figure 11, $\Phi_{ee}(r)$ for all three fusion reactions have the same value, but in Figure 12, $P^{11}B$ has the maximum value of $\Phi_{ii}(r)$, then D^3He, and finally DT.

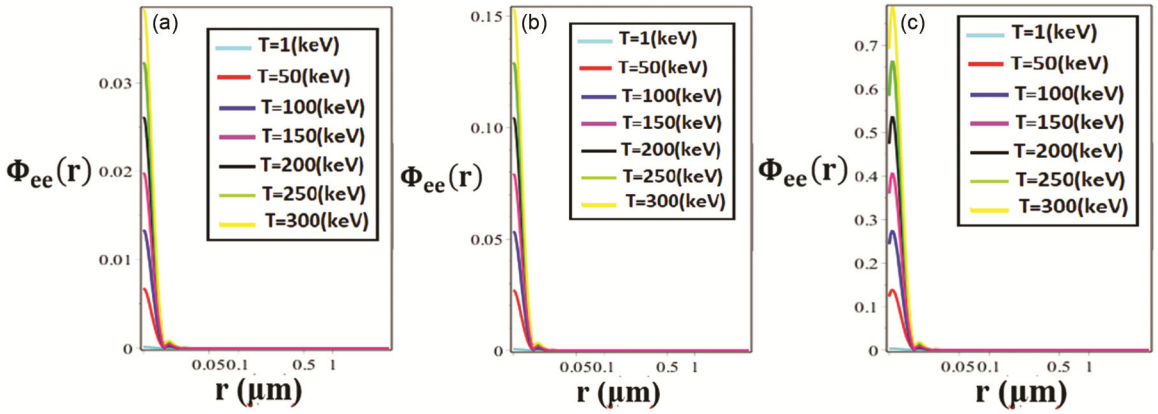

Fig. 12 — variations of $\Phi_{ii}(r)$ (ion-ion effective interaction potential) as a function of r and T for three fusion reactions: a) DT, b) D^3He, and c) $P^{11}B$ in the range of $0 \le r(\mu m) \le 4$ and $1 \le T(keV) \le 300$

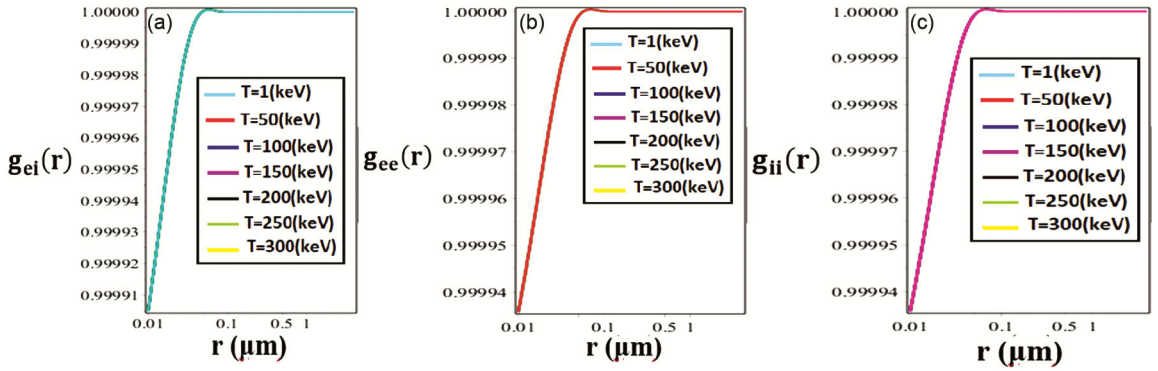

Fig. 13 — variations of (a) $\mathbf{g_{ei}(r)}$ (electron-ion pair correlation function), (b) $\mathbf{g_{ee}(r)}$ (electron-electron pair correlation function), and (c) $\mathbf{g_{ii}(r)}$ (ion-ion pair correlation function) as a function of r and T in the range of $0 \le r(\mu m) \le 4$ and $1 \le T(keV) \le 300$.

4.2 Thermodynamical Properties of Dense Plasma in ICF

Based on the effective interaction potentials, the pair correlation functions with exponential approximation are given by:

$$g_{\alpha\beta}(r) = \exp\left(-\frac{\Phi_{\alpha\beta}(r)}{k_B T_{\alpha\beta}}\right) \quad \dots (15)$$

Where, $\Phi_{\alpha\beta}(r)$ is the effective interaction potential of α and β particles. Figure 13 shows the variations of a) $g_{ei}(r)$ (electron-ion pair correlation function), b) $g_{ee}(r)$ (electron-electron pair correlation function), and c) $g_{ii}(r)$ (ion-ion pair correlation function) as a function of r and T in the range of $0 \le r(\mu m) \le 4$ and $1 \le T(keV) \le 300$.

The results of our calculations as shown in Figure 13 show that the variations of electron-ion pair correlation function ($g_{ei}(r)$) and electron-electron pair correlation function ($g_{ee}(r)$) and ion-ion pair correlation function ($g_{ii}(r)$) according to the interaction distance r and the temperature T(keV), is a fixed value at different temperatures and has almost the same value for all three fusion reactions mentioned. Pressure, P, and energy, E, are thermodynamical properties of plasma and are obtained through pair correlation functions and effective interaction potential such that are determined by equations (16) and (17), respectively [34]:

$$P = P_{id} - \frac{2}{3}\pi \sum_{a=i.e} n_a \sum_{b=i.e} n_b \int_0^{\infty} \frac{\partial \Phi_{a.b}(r)}{\partial r} g_{a.b}(r) r^3 dr \quad \dots (16)$$

$$E = E_{id} - \pi \sum_{a=i.e} n_a \sum_{b=i.e} n_b \int_0^{\infty} \Phi_{a.b}(r) g_{a.b}(r) r^2 dr \quad \dots (17)$$

In Table 1, we have made a comparison between the numerical values of thermodynamical properties P and E of the fusion plasma obtained from the Eqs (16) and (17) for the three fuels D^3He and $P^{11}B$.

From the calculated numerical values, we find that with increasing the temperature for the three fusion reactions of DT, D^3He and $P^{11}B$, the pressure (P) and energy (E) increase, such that the maximum values of P are belong to $P^{11}B$, D^3He and finally DT,

Table 1 — Comparison of the numerical values of the thermodynamic properties of P and E of the fusion plasma obtained from the calculations of the Eqs (16) and (17) for the three fuels DT, D^3He and $P^{11}B$ in the range of $0 \le r(\mu m) \le 4$ and $1 \le T(keV) \le 300$

	DT	DT	D^3He	D^3He	$P^{11}B$	$P^{11}B$
T(keV)	P(Gpa)	E(MeV)	P(Gpa)	E(MeV)	P(Gpa)	E(MeV)
50	280	1.53	400	2.50	480	4.10
100	570	3.22	620	4.52	670	8.22
150	880	4.82	895	7.31	898	12.46
200	989	6.51	967	9.92	975	16.37
250	1010	8.12	1013	12.43	1035	20.63
300	1077	9.70	1082	14.95	1093	25.32

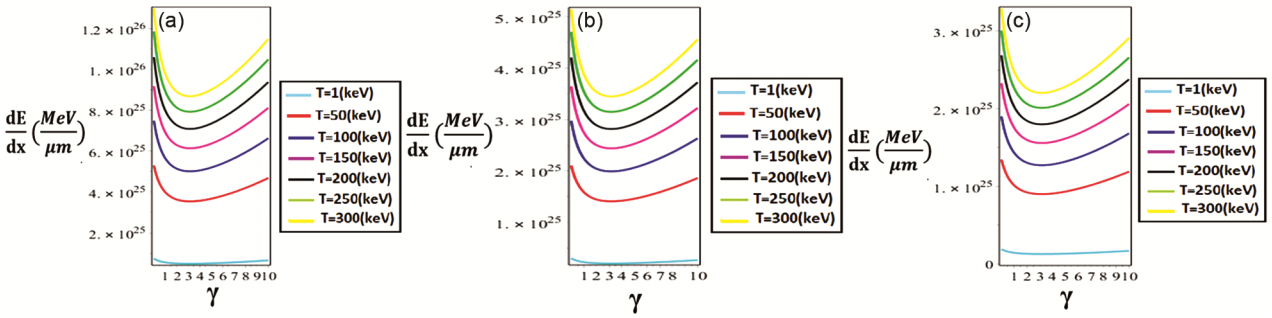

Fig. 14 — variations of $\frac{dE}{dx}(\frac{MeV}{\mu m})$ (stopping power) as a function of γ and T for three fusion reactions: a) DT, b) D^3He, and c) $P^{11}B$ in the range of $0.01 \le \gamma \le 10$ and $1 \le T(keV) \le 300$

respectively, while the maximum value of E are belong to DT, $P^{11}B$ and finally D^3He, respectively. These thermodynamic relationships are used to solve the Huguenot equation [35]:

$$H(V.P.E) = E - E_0 + {}^1/_2\,(V - V_0)(P + P_0) = 0 \quad \ldots (18)$$

where $P_0 = 0$ and $\rho_0 = 0 \cdot 171\,\frac{g}{cm^3}$ and $E_0 = -15 \cdot 886\,\frac{eV}{atom}$. In fact, E_0, V_0 and P_0 are the initial energy, the initial volume and the initial plasma pressure, respectively, while E, V and P, are final energy, final volume and final plasma pressure, respectively.

4.3 Dynamical Properties of Dense Plasma in ICF

One of the important parameters to describe the interaction of ions with materials is the energy of the projectile. The stopping power is a parameter that determines the average energy loss of fast electrons or ions in the plasma and is determined by Eq (19):

$$\frac{dE}{dx} = 8\pi n\left(\frac{\mu_{\alpha\beta}}{m_\beta}\right) E_c b_\perp^2 \Lambda_{\alpha\beta} \quad \ldots (19)$$

where $E_c = {}^1/_2\, m_{\alpha\beta} v^2$ is the energy of the center of mass, v is the relative velocity of the scattered particle, $\Lambda_{\alpha\beta}$ is Coulomb's logarithm and $b_\perp$ is the collision parameter, which is determined by: $b_\perp = (Z_\alpha Z_\beta e^2)/2E_c$.[36,37] In Fig. 14, we plotted the variations of dE/dx (stopping power) in terms of γ and T(keV) for three fusion reactions a) DT, b) D^3He, and c) $P^{11}B$ in the range of $0.01 \le \gamma \le 10$ and $1 \le T(keV) \le 300$,respectively.

From the graphs in Fig. 14, it is clear that the changes in the stopping power (dE/dx) for the three fusion reactions DT, D^3He and $P^{11}B$ in terms of Lorentz coefficient γ and temperature T(keV), increase with increasing temperature and with increasing γ, first increase and then decreases and D^3He has the highest dE/dx value, followed by $P^{11}B$ and finally DT. The Coulomb logarithm is determined based on the effective interaction potential of particles through the scattering angle of the pair Coulomb collision. By introducing the center of mass in the collision process, the Coulomb logarithm is written as Eq (20)[38,39]:

$$\Lambda_{\alpha\beta} = \frac{1}{b_\perp^2}\int_0^{b_{max}} \sin^2\left(\frac{\theta_c}{2}\right)\cdot bdb \quad \ldots (20)$$

where, $b_{max} = r_D$ is the maximum impact parameter. The scattering angle of the center of mass can be obtained from the well-known formula (21):

$$\theta_c = \pi - 2b\int_{r_0}^{\infty}\frac{dr}{r^2}\left(1 - \frac{\Phi_{\alpha\beta}(r)}{E_c} - \frac{b^2}{r^2}\right)^{-1/2} \quad \ldots (21)$$

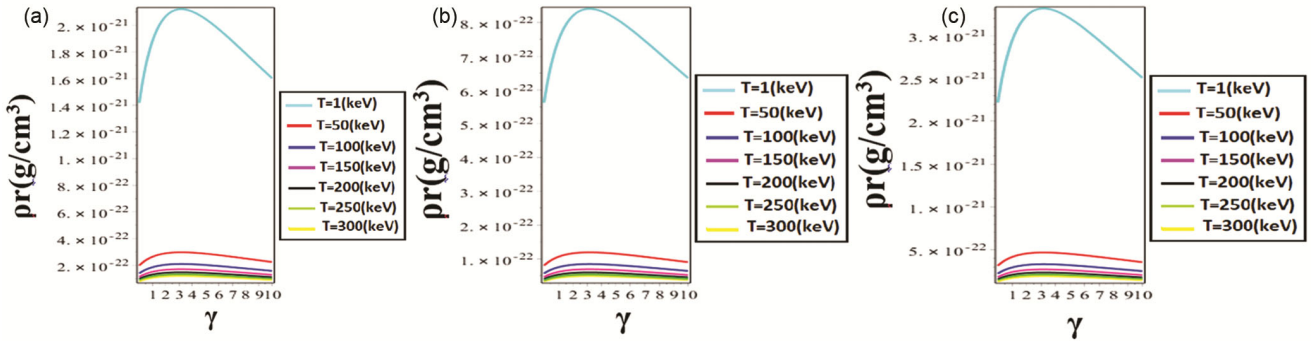

Fig. 15 — variations of ρr(g/cm^3) (particle range) as a function of γ and T for the three fusion reactions: (a) DT, (b) D^3He, and (c) $P^{11}B$ in the range of 0·01≤γ≤10 and 1≤T(keV)≤300.

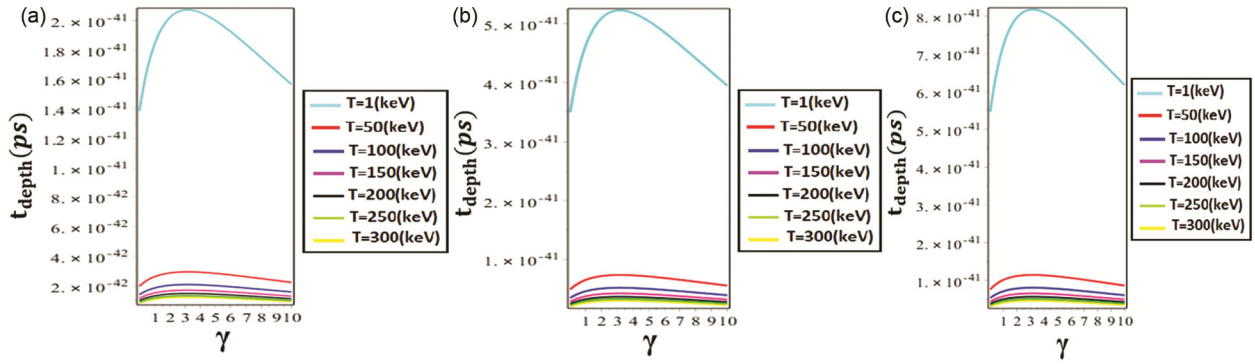

Fig. 16 — variations of $t_{depth}(ps)$ (stopping time) as a function of γ and T for three fusion reactions: a) DT, b) D^3He, and c) $P^{11}B$ in the range of $0.01 \le \gamma \le 10$ and $1 \le T(keV) \le 300$

In Eq (21), $\Phi_{\alpha\beta}(r)$ is the effective interaction potential and r_0 is the distance of the closest path for the impact parameter b. In fusion reactions, to absorb the energy of α particles, the size of the fuel must be greater than the range ρr. This range of particles is obtained by Eq (22) and Fig.15 shows the variations of ρr (particle range) in terms of γ and T for three fusion reactions a) DT, b) D^3He, and c) $P^{11}B$ in the range of 0·01≤γ≤10 and 1≤T(keV)≤300:

$$\rho r = \int_E^{E_0} \left(\frac{dE}{\rho dx}\right)^{-1} dE \qquad \ldots (22)$$

In this relation, E_0 is the initial energy of the particles. It should be noted that this range is expressed in terms of $(\frac{g}{cm^2})$. For a more accurate description of thermonuclear fusion, parameters such as the average scattering angle, $\langle\cos\theta\rangle$, stopping time,$t_{depth}$and ion penetration depth,ρx should also be introduced. The stopping time of ions in the plasma is determined by Eq (23) and Fig.16 shows the variations of t_{depth} (stopping time) in terms of γ and T for three fusion reactions a) DT, b) D^3He, and c) $P^{11}B$ in the range of $0.01 \le \gamma \le 10$ and $1 \le T(keV) \le 300$, respectively.

$$t_{depth} = \int_E^{E_0} \left(\frac{dE}{dt}\right)^{-1} (dE) \qquad \ldots . (23)$$

Also, from the calculations we have done to determine ρr and stopping time (t_{depth}) for three fusion reactions DT, D^3He and $P^{11}B$ in terms of Lorentz coefficient γ and temperature T, it is concluded that these graphs have a similar behavior, i.e., reduced at different temperatures But with the increase of γ, they first increase and then decrease, and the maximum value of ρr at first is belong to D^3He, then $P^{11}B$, and finally DT, and the maximum value of t_{depth} at first is belong to $P^{11}B$, then D^3He, and finally DT. The penetration depth of plasma particles with the initial energy of E_0 can also be calculated using Eq (24) and Fig. 17 shows the graphs of ρx (penetration depth) in terms of γ and T for three fusion reactions a) DT, b) D^3He, and c) $P^{11}B$ in the range of 0.01≤γ≤10 and 1≤T(keV)≤300, respectively:

$$\rho x = \int_E^{E_0} \langle\cos\theta\rangle \left(\frac{dE}{\rho dx}\right)^{-1} dE \qquad \ldots (24)$$

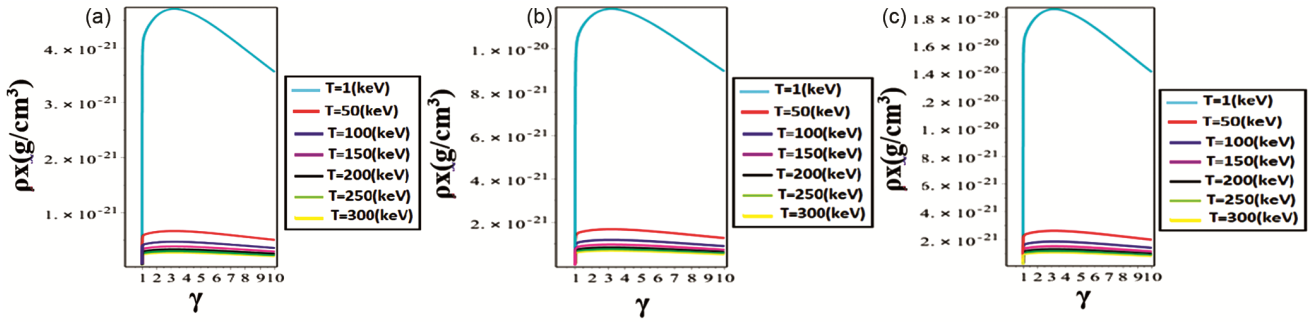

Fig. 17 — variations of the ρx(g/cm^3) (penetration depth) as a function of γ and T for three fusion reactions: (a) DT, (b) D^{3}He, and (c) P^{11}B in the range of $0.01 \leq \gamma \leq 10$ and $1 \leq T(keV) \leq 300$

According to Fig. 17, the calculations show that the changes in range or penetration depth (ρx) for the three fusion reactions DT, D^{3}He and P^{11}B in terms of Lorentz coefficient γ and temperature T, at different temperatures, decreased, but with the increase of γ, ρx increased. and at $1 \simeq \gamma$ it reaches its maximum value and has a decreasing trend and the highest value of ρx at first is belong to P^{11}B, then DT and finally D^{3}He.

5 Conclusion

Thermodynamical relationships calculated based on the effective interaction potential, which includes collective effects and quantum mechanical effects, have been used to obtain the solution of the Huguenot equation. The stopping time depends on the initial energy values, density and temperature of the fuel. The effect of temperature on the average deviation angle is more important than the effect of temperature on the density of particles. The development of the method of effective interaction potentials is important because it provides a deeper understanding of the physics of dense plasmas. It can also provide fast and accurate calculations for changes in various physical properties. Therefore, the issues mentioned above need to be addressed in future works.

In general, in this work we were able to find the thermodynamical properties of the three fusion plasma parameters DT, D^{3}He, and p^{11}B in terms of temperature, distance, and Lorentz factor. The results of our calculations show that the calculated parameters in our work for the DT fusion fuel are in good agreement with the results of other groups, which shows the validity of our research work. While for the parameters belong to D^{3}He and p^{11}B fuels no references were found for comparison, because they have been studied for the first time by the authors of this article. It is hoped that this work can be a foundation for further research of these fuels without neutrons.

References

1 Cohen S A & Glasser A H, *Phys Rev Lett*, 85 (2000) 5114.
2 Cohen S A, Berlinger B, Brunkhorst C, Brooks A, Ferraro N, Lundberg D P, Roach A & Glasser A H, *Phys Rev Lett*, 98 (2007) 145002.
3 Alam F, Sarkar R & Chowdhury H, *Energy Procedia*, 160 (2019) 3.
4 Alhamdan A, Halem Z, Hernandez I, Lo A W, Singh M, & Whyte D, Financing fusion energy, (2022) available at SSRN 4301605.
5 Cohen S. A, Swanson C, McGreivy N, Raja A, Evans E, Jandovitz P, Khodak M, Pajerj G, *J British Interplanetary Soc*, 72 (2019) 37, https://collaborate.princeton.edu/en/publications/direct-fusion-drive-for-interstellar-exploration.
6 Genta G & Kezerashvili R Y, *Acta Astronautica*, 173 (2020) 303.
7 Gajeri M, Aime P, Roman & Kezerashvili Ya, *Acta Astronautica*, 180 (2021) 429.
8 Gajeri R & Kezerashvili Ya, *Acta Astronautica*, 178 (2021) 257.
9 Zhiyuan C, Yibai W, Min L C, Peng W, Yimeng W, Siyu L, Guangchuan Z, Junxue R, Haibin T, *Astronautica*, 2010 (2023) 82.
10 Zylstra A, Kritcher A, Hurricane O, Callahan D, Ralph J, Casey D, *et al.*, *Phys Rev E,* 106 (2022) 025202.
11 McCrory R, Bahr R, Betti R, Boehly T, Collins T, Craxton R, *et al.*, *Nucl Fusion*, 41 (2001) 1413.
12 Shiraga H, Fujioka S, Nakai M, Watari T, Nakamura H, Arikawa Y, *et al.*, *Plasma Phys Control Fusion* 53 (2011) 124029.
13 Fujioka S, Zhang Z, Ishihara K, Shigemori K, Hironaka Y, Johzaki T, *et al.*, *Laser Sci Rep*, 3 (2013) 1.
14 Belyaev V, Matafonov A, Vinogradov V, Krainov V, Lisitsa V, Roussetski A *et al., Phys Rev E* 72 (2005) 026406.
15 Margarone D, Bonvalet J, Giuffrida L, Morace A, Kantarelou V, Tosca M, *et al.*, *Laser Appl Sci*, 12 (2022)1444.
16 Willingale L, Petrov G, Maksimchuk A, Davis J, Freeman R, Joglekar A, *et al., Phys Plasmas*, 18 (2011) 083106.
17 Hora H, Korn G, Giuffrida L, Margarone D, Picciotto A, Krasa J, *et al., Laser Part Beams*, 33 (2015) 607.
18 Hora H, Eliezer S, Kirchhoff G, Nissim N, Wang J, Lalousis P, *et al.*, *Laser Part Beams* 35 (2017) 730.
19 Spitzer L, Physics of Fully Ionized Gases, Interscience Tracts on Physics and Astronomy, 2nd rev ed, (1962), https://books.google.com/books/about/Physics_of_Fully_Ionized_Gases.html?id=CilRAAAAMAAJ.

20 Trubnikov B, *Review of Plasma Physics* (1965).
21 Skupsky S, *Phys Rev A*, 16 (1977) 727.
22 Li C K &Petrasso R D, *Phys Rev Lett*, 70 (1993) 3059.
23 Lindl J. D. (1998). Inertial Confinement Fusion: The Quest for Ignition and Energy Gain Using Indirect Drive; references therein
24 Tabak M et al., *Phys. Plasmas* 1 (1994) 1626.
25 Honda M, Meyer-ter-Vehn J & Pukhov A, *Phys Rev Lett*, 85 (2000) 2128.
26 Rosen M D *et al*. *Phys Rev A*, 36 (1987) 247.
27 Jacobi B, Stoeckl C, Boehly T, Meyerhofer D D & Seka W, *Phys Plasmas* 7 (2000) 3714.
28 Deutsch C, *et al*. *Phys Rev Lett*, 77 (1996) 2483.
29 Hughes P A, ed. Beams and Jets in Astrophysics, Cambridge Astrophysics Series (1991).
30 Pukhov A, Sheng Z M & Meyer-ter-Vehn J, *Phys Plasmas*, 6 (1999) 2847.
31 Lewis H W, *Phys Rev*, 78 (1950) 526.
32 Goudsmit S & Saunderson J L, *Phys Rev*, 57 (1940) 24.
33 Kodanova S K, Ramazanov T S, Issanova M K, Nigmetova G N & Moldabekov Zh A, *Contrib Plasma Phys*, 55 (2015) 271.
34 Levashov P R, Bonitz M, Filinov V S & Fortov V E, *J Phys A*, 39 (2006) 4447.
35 Ordonez C A & Molina M I, *Phys Plasmas*, 1 (1994) 2515.
36 Ramazanov T S & Kodanova S K, *Phys Plasmas*, 8 (2001) 5049.
37 Belyaev G, Basko M, Cherkasov A, Golubev A, Fertman A, Roudskoy I, Savin S, Sharkov B, Turtikov V, Arzumanov A, Borisenko A, Gorlachev I, Lysukhin S, Hoffmann D H H & Tauschwitz A, *Phys Rev E*, 53 (1996) 2701.
38 Ramazanov T S, Kodanova S K, Moldabekov Zh A & Issanova M K, *Phys Plasmas*, 20 (2013) 112702.
39 Mahdavi M & Koohrokhi T, *Phys Rev E*, 85 (2012) 016405.